HHS Public Access

Author manuscript

Adv Funct Mater. Author manuscript; available in PMC 2022 July 23.

Published in final edited form as:

Adv Funct Mater. 2021 July 23; 31(30): . doi:10.1002/adfm.202101638.

Nanowire Assisted Mechanotyping of Cellular Metastatic Potential

Debadrita Paria[#1], **Annalisa Convertino**[#2], **Piyush Raj**[1], **Kristine Glunde**[5], **Yun Chen**[1,3,4], **Ishan Barman**[1,5,6,*]

[1]Department of Mechanical Engineering, Johns Hopkins University, Baltimore, MD, USA

[2]Institute for Microelectronics and Microsystems, National Research Council, Roma, Italia

[3]Institute for NanoBioTechnology, Johns Hopkins University, Baltimore, MD, USA

[4]Center for Cell Dynamics, Johns Hopkins University, Baltimore, MD, USA

[5]Department of Oncology, Johns Hopkins University School of Medicine, Baltimore, MD, USA

[6]Department of Radiology & Radiological Science, Johns Hopkins University School of Medicine, Baltimore, MD, USA

[#] These authors contributed equally to this work.

Abstract

Nanotechnology has provided tools for next generation biomedical devices which rely on nanostructure interfaces with living cells. *In vitro* biomimetic structures have enabled observation of cell response to various mechanical and chemical cues, and there is a growing interest in isolating and harnessing the specific cues that three-dimensional microenvironments can provide without the requirement for such culture and the experimental drawbacks associated with it. Here we report a randomly oriented gold coated Si nanowire substrate with patterned hydrophobic-hydrophilic areas for differentiation of isogenic breast cancer cells of varying metastatic potential. When considering synthetic surfaces for the study of cell-nanotopography interfaces, randomly oriented nanowires more closely resemble the isotropic architecture of natural extracellular matrix as compared to currently more widely used vertical nanowire arrays. In the study reported here, we show that primary cancer cells preferably attach to the hydrophilic region of randomly oriented nanowire substrate while secondary cancer cells do not adhere. Using machine learning analysis of fluorescence images, cells were found to spread and elongate on the nanowire substrates as compared to a flat substrate, where they mostly remain round, when neither surface was coated with extracellular matrix (ECM) proteins. Such platforms can not only be used for developing bioassays but also as stepping stones for tissue printing technologies where cells can be selectively patterned at desired locations.

Graphical abstract

[*]**Correspondence:** Ishan Barman, Johns Hopkins University, Whiting School of Engineering, Department of Mechanical Engineering, Latrobe Hall 103, Baltimore, MD 21218, USA, ibarman@jhu.edu.

Conflict of Interest: The authors disclose no potential conflicts of interest.

In vitro biomimetic structures permit direct observation of cell response to mechanical cues that are similar to those in the native tissue microenvironments. Here, we employ randomly oriented gold coated silicon nanowires with patterned hydrophobic and hydrophilic regions to reveal the strikingly different adhesion patterns for primary breast cancer cells and their metastatic derivatives on such surfaces. The developed nanopatterned platform offers a new route towards mechanotyping of cancer cells, paving the way for future diagnostic assays for quantification of metastatic propensity of patient samples.

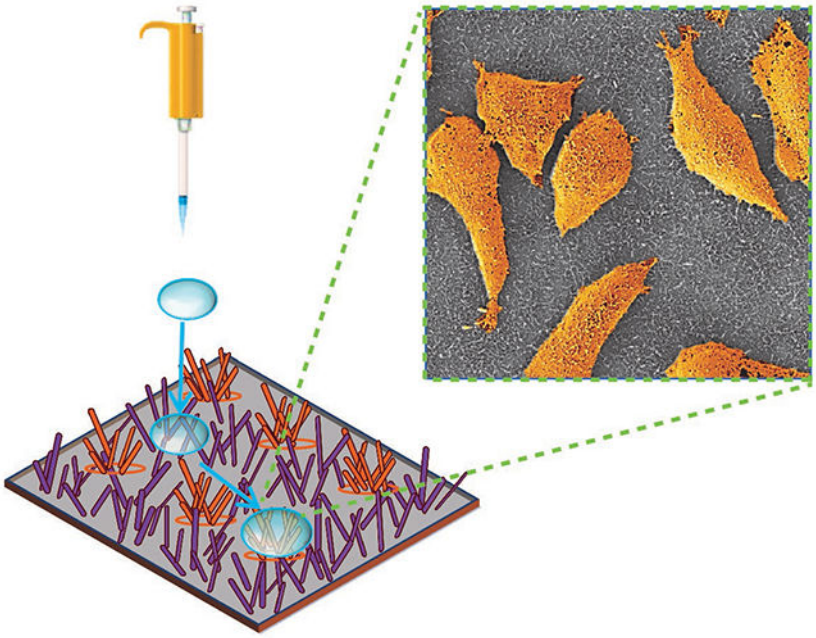

Keywords

Metastatic cells; silicon nanowires; hydrophilic-hydrophobic surface; microfabrication; machine learning

INTRODUCTION

Important cellular functions like adhesion, migration, regeneration, apoptosis, proliferation, polarization, among others are influenced by the mechanical cues provided by extracellular matrix (ECM), the non-cellular tissue component surrounding the cell [1–5]. Basement membranes, the ECM layer underlying the basal side of the epithelium, contains fibrillar proteins such as laminin and fibronectin and non-fibrillar protein like collagen IV, forming a complex three-dimensional (3D) topography of nanoscale dimensions [6,7]. Pioneering works based on simple and ordered arrangements of nanoscale features demonstrate that 3D nano-architectures contribute to cellular morphology, differentiation and growth [8–10]. Nanotechnology has provided the opportunity to artificially create complex nanostructures that better represent the complex physiological microenvironment [11–13] beyond orderly organization, allowing the reconstitution of particular cellular phenotypes *in vitro*. Mammalian cells show similar interactions with synthetic topography prepared

by micro/nano fabrication technology [12,14,15], which allows for exploring various applications ranging from bio-sensing and drug delivery to fundamental understanding of cellular communications and processes.

It is worth noting that it is not the mere increase of dimensionality, but the functional consequences that arise from the finer architectures of different topographies that influence the cellular functions [16]. In a pursuit to isolate and harness the specific cues that 3D microenvironments provide without the requirement for 3D culture and the accompanying experimental drawbacks, notably non-optimal imaging and interdependent microenvironmental factors, micro- and nanopatterned substrates have gained significant attention. For instance, while micropatterned surfaces have been used to precisely control cell adhesion and spreading [17,18], nanoscale gratings have been leveraged to restrict the movement and clustering of specific receptors to alter signaling from these receptors [19].

Along with surface topography, surface chemistry [20,21] and wettability [22,23] play an important role in regulating cellular phenotypes and behaviors. Specifically, cell morphology and adhesion have a strong correlation with the wettability of a surface [24]. Increased or decreased contact area of cells in solution on a surface influences cell shape and strength of cell-substrate adhesion, resulting from the hydrophilic or hydrophobic nature of this surface. The cytoskeleton, a dynamic supramolecular structure governing important cellular functions, adapts its organization to accomplish force balance between the cell and the surface. Surface wettability determines how much of the surface is exposed to culture media leading to adsorption of adhesive cellular proteins. Lower interfacial tension between the liquid and the substrate surface may lead to less adsorption of adhesion-mediating proteins, resulting in adhesion failures for cells [24]. Thus, along with nanotopography, surface wettability is an important consideration to determine cell surface interactions.

Among various topographies in the size range that closely mimic natural ECM fibrils [25,26], vertical nanowire-based systems have been one of the most widely explored architectures for studying cellular behavior [27,28], probing intracellular biomolecular changes [29,30] or in situ drug [31] or gene delivery [32]. Vertical nanowire-assisted intracellular neural recording [33,34] and piconewton force measurement in neural growth cones [35] have been reported. Nanowires combined with transistors have been used for biosensing applications [36]. Modulation of cell adhesion by super hydrophobic and hydrophilic surfaces [37] has been utilized for cell patterning in bioassay [38]. Micropatterning of cells was enabled by a combination of topography and super hydrophilicity, allowing cells to concentrate on the hydrophilic region [39].

While most prior studies on cell-nanostructure interfaces have been based on vertical nanowires, to the best of our knowledge, there are no other studies related to the cell-surface interactions of randomly oriented nanowires, which better resemble naturally occurring ECM organization [40,41]. Here we report a novel substrate with swaths of randomly oriented hydrophobic- hydrophilic gold-coated silicon nanowires (Au/SiNWs) to sort human breast cancer cells of different stages of metastatic progression. In addition to advantages which include high yield, low cost and facile fabrication, randomly oriented Au/SiNWs are cyto-compatible with mammalian cells [42,43]. Moreover, their large surface-to-volume-

ratio enables greater cell-surface interactions, which allow for sensing and probing of cellular function by electrical and optical means [42–44]. The spreading, elongation and concentration of primary tumor cells on the hydrophilic nanowire surface without any protein coating demonstrates the potential of a robust biomimicry platform for tissue printing applications. Surprisingly, secondary cancer cells isolated from lung and bone metastases do not/minimally adhere to either the hydrophilic or the hydrophobic region of the Au/SiNWs substrate. This paves the way for nanowire-based bioassays for diagnosing and monitoring tumor progression.

RESULTS AND DISCUSSION

Randomly oriented SiNWs were obtained by plasma enhanced chemical vapor deposition (PECVD) on silicon (Si) wafer and successively coated with gold (thickness of 120 nm) by thermal evaporation.

The forest of Au/SiNWs is intrinsically highly hydrophilic and was converted to super-hydrophobicity by treatment with plasma of fluorocarbon (CHF_3) for 90 s (details in Materials and Methods). Figure 1(A) shows photographs of the wettability difference between the untreated (left) and treated area (right) on the same Au/SiNWs substrate. The two regions with different wettability were obtained by using a contact mask that protected half of the sample during fluorocarbon treatment. The water droplet on the uncoated region was well spread, wetting a large area of the surface, while on the other side, the droplet sitting on the treated region showed a contact angle of 155° (figure 1 (B)) suggesting super-hydrophobicity of the area after fluorocarbon treatment. Figure 1 (C) and (D) depict the scanning electron microscope (SEM) images of the Au/SiNWs before and after fluorocarbon treatment. These images reveal that for both untreated and treated samples, the morphology of the Au/SiNWs remain similar, consisting of a dense ensemble of disordered and randomly oriented NWs which are around 2-3 μm long, with an average diameter of about 120–150 nm.

Before introducing the Au/SiNW substrate into cell culture, a micro-pattern consisting of hydrophobic-hydrophilic regions was fabricated on the NW mat by using a two-step process as summarized in figure 2(A). First, the AuSiNW surface was modified through fluorocarbon plasma to achieve hydrophobic properties (figure 2(A), 2). Next, the hydrophobic-hydrophilic micro-pattern was fabricated by selective removal of fluorocarbon coverage using an oxygen (O_2) plasma-based process through reactive ion etching (RIE) (figure 2(A), 4). To pattern the hydrophilic regions, a shadow mask (24 circular holes with a size and a separation of 500 μm each) was placed in contact with the sample. For a practical demonstration of the selective hydrophobic–hydrophilic patterning, we dispensed water droplets on the patterned substrate which resulted in the droplets rolling off hydrophobic regions and preferentially settling on hydrophilic regions (figure 2(B)). Adherent cells have an affinity towards hydrophilic surfaces [39]. Thus, in biological contexts, it is expected that cells will tend to grow and concentrate preferentially on hydrophilic regions.

Two different cell lines, parental human breast cancer cells MDA-MB-231 (P231) and lung-metastatic cells (LM231), which were derived from P231 in an orthotopic mouse

tumor xenograft model in which LM231 was isolated from spontaneous lung metastases [45], were tested in our study alongside a third bone-selective metastatic derivative MDA-MB-231-1833 (BoM). Our recent investigations had revealed distinct differences in the biophysical and morphological properties of the P231 and LM231 cells. Briefly, LM231 cells were found to be more motile and less stiff, highlighting their invasiveness as compared to P231 cells [46]. Furthermore, LM231 cells displayed a larger area and higher cell mass as compared to P231 cells [47]. Based on these recent findings, we sought to investigate if P231, LM231 and BoM cells would interact differently with the hydrophobic-hydrophilic nanowire substrate.

Constitutively tdTomato-expressing P231 and LM231 cells were cultured on the substrate with patterned Au/SiNWs areas. BoM cells were also cultured on the patterned substrate. In the same dish a flat silicon wafer was placed as a control surface at the same time. None of the substrates were modified with collagen or poly-L-lysine, which are known cell adhesion promoters. The culture protocol is provided in the Materials and Methods.

The substrates were fixed 48 hours after plating and observed using a fluorescence microscope. The fluorescence image of hydrophobic-hydrophilic Au/SiNWs seeded with P231 cells (figure 3(A)) shows that the cells grew on the hydrophilic portion of the pattern at high density (lower right corner), whereas cells were nearly absent from the hydrophobic section (upper left corner). A minimum number of LM231 and BoM cells, on the other hand, were observed in the hydrophilic circles (upper right corner of figure 3(B) and upper left corner of figure 3(C), respectively) and could not be found at all on the hydrophobic side (lower left corner and right corner). Uniform distributions of P231, LM231 and BoM cells were observed on Si wafer (figure 3(D), 3(E) and 3(F), respectively) confirmed that cells were uniformly dispersed in the solution prior to plating. These findings support the notion that the observed differential adhesion resulted from combined effects of substrate topography and wettability.

ECM remodeling in the primary tumor microenvironment is strongly correlated with metastatic progression [48,49]. Biochemical and biophysical changes occur in the ECM in close proximity to the tumor, leading to metastasis. For example, increased protein deposition [50] and increased stiffness of the ECM [51] were found to contribute to primary tumor progression. However, the engrafted cancer cells have poor efficiency of forming a secondary tumor owing to the unfavorable microenvironment at the distant site [52], often requiring local cells at the invaded site to secrete additional ECM proteins to facilitate colonization [53]. Such difference suggests that cell-ECM interaction of primary cancer cells may be different than that of secondary cancer cells, which is in agreement with our observation on Au/SiNWs.

A closer inspection of the fluorescence images reveals that the morphology of P231 cells grown on the hydrophilic Au/SiNW *versus* that on the planar substrate were different from each other. Although neither substrate was coated with collagen or poly-L-lysine, P231 adhered to and grew on both. However, fluorescence images show that P231 on the hydrophilic Au/SiNWs (figure 4(A)) exhibited 1.872-fold greater spreading and 1.39-fold more elongation compared to that of cells grown on control Si (figure 4(B)). SEM of

dried P231 cells on the hydrophilic Au/SiNWs (figure 4(C)) and flat Si wafer (figure 4(D)) confirmed these findings. The cells grew on both surfaces indicating that they were healthy and the difference in morphology was promoted by the nanostructuring of the Au/SiNWs. Similar observations have been reported earlier, where cells were grown and elongated along the ridges of nanostructured grooves [54–56]. Some other studies report opposite observations [57] indicating strong dependence of the observed phenomenon on cell type and surface modifications [26,58].

To further characterize the differential morphologies based on the substrate, we used VAMPIRE (Visually Aided Morpho-Phenotyping Image Recognition) analysis [59,60] to elucidate subtle differences within cell morphologies. Frequently, cell shapes vary greatly while keeping broad morphological parameters such as area and aspect ratio preserved. VAMPIRE analysis helped us to tease out the subtle differences in cell shapes while ensuring high throughput of the approach. For the analysis, fluorescence images were pooled to collect more than 1,500 and 2,000 P231 cells on Au/SiNWs and Si wafer, respectively. The histogram in Figure 4(E) and 4(F) depicts the percentage of different shape modes for each condition. Dendrogram of representative shape modes is shown in figure 4(G). Approximately 50% of the cell shape was elongated with a circularity of 0.66 on Au/SiNWs, whereas round shapes (circularity: 0.87) were dominant in the case of flat surfaces. Furthermore, although it is outside the scope of our current study, our observations indicate that the degree of surface roughness may also play a role in determining cellular morphology on such substrates (Supporting Information).

Finally, we assessed the viability of the P231 cells on hydrophilic Au/SiNWs. At 24 hours post seeding, cells on Au/SiNWs and plain Si wafer were stained to assay for live and dead cells. For the live cell assay, Calcein AM diluted in PBS was used. To probe dead cells, we used Hoechst 33342, which stains nuclei regardless of whether cells are alive or dead. Cells stained with Hoechst only were dead. The percentage of live and dead cells were assessed using ImageJ as shown in Figure 5(A) and 5(B). Figure 5(C) quantitatively displays the percentage of live and dead cells on Au/SiNWs as compared to Si wafer. Au/SiNWs had a slightly reduced live-to-dead ratio (81.6% live cells) as compared to Si (96.3% live cells). The slightly lower survival rate of cells on Au/SiNWs *versus* Si may have been caused by the complex topography of Au/SiNWs substrate, where dead cells may have been retained on its surface. Overall, 81.6% cell survival on Au/SiNWs substrate suggests that it is intrinsically inert and does not impose cytotoxicity on cells.

CONCLUSION

In this report, we demonstrate a patterned hydrophobic-hydrophilic Au/SiNWs platform that is able to differentiate isogenic breast cancer cells of two different stages of metastatic progression. The primary cancer cells remained alive and selectively adhered to the hydrophilic region of the nanowire substrate. Furthermore, the cells exhibited distinct morphologies on Au/SiNWs compared to their counterparts on a flat surface, indicating that randomly oriented nanowire substrates can be used to modulate cellular phenotypes. With further development, such platforms can be used in synthetic biology or for tests to evaluate the metastatic capacity of cancer cells. Chemical functionalization or integration with

plasmonically active materials can provide added functionality to the nanowire platform for detailed mechano-chemical studies in the future.

Materials & Methods

Fabrication of Au/SiNWs

Au catalyzed SiNWs were produced by plasma enhanced chemical vapor deposition (PECVD) on Si wafer. To initiate NW growth, a 2 nm thick Au film was evaporated on the substrate. SiNW growth was performed with SiH_4 and H_2 as precursors at a total pressure of 1 Torr and flow ratio of $SiH_4/(H_2+SiH_4)$ fixed to 1:10. The substrate temperature was kept constant at 350°C. A 13.6 MHz radiofrequency with a fixed power of 5 W was used to ignite the plasma. The Au coverage on the SiNWs was obtained by thermal evaporation.

Fabrication of hydrophobic-hydrophilic surface on substrate with Au/SiNWs

The micro-pattern consisting of hydrophobic-hydrophilic surface regions was fabricated on Au/SiNW substrates by using a two-step process. First, to obtain a hydrophobic surface the Au/SiNW substrate was exposed to a plasma of fluorocarbon (CHF_3) and Ar for 90 s at a total pressure of 100 mTorr and a flow ratio of CHF3/(CHF3+Ar) fixed to 60%, at room temperature and RF power of 50 W[61]. Next, the hydrophilic-hydrophobic micro-pattern was fabricated by selective removal of fluorocarbon coverage using an oxygen plasma-based process through a reactive ion etching (RIE) technique. To select hydrophilic regions, we used a shadow mask in contact with the sample that had a matrix of 24 circular holes with a size and a separation of 500 μm each.

Cell culture on the Au/SiNWs

10% fetal bovine serum (Corning Cellgro), 100 U/mL of penicillin were added to RPMI 1640 with L-glutamine (Corning Cellgro) prior to use for culturing P231 and LM231 cells. MDA-MB-231-1833 bone-selective metastatic derivative, BoM, was kindly provided by Dr. Joan Massagué (Memorial Sloan Kettering; New York, NY) [62]. For these cells, DMEM media was used instead of RPMI as per the provider's recommendation. The cultures were maintained in a humidified sterile environment in the presence of 5% CO_2 at 37°C. Trypsin-EDTA was used to detach the cells from the cell culture dish and for seeding them at a density of approximately 10^6 onto the substrate in a 60-mm culture dish. Au/SiNWs were exposed to UV light for 24 hours for sterilization and dipped in cell culture media for a few minutes prior to adding cells.

For fixing the cells, substrate was washed with PBS at room temperature twice before it was immersed in formalin for 15 minutes. Post fixation the substrate was washed again with PBS and stored in the same solution for imaging.

SEM sample preparation

The cells on the substrate were gradually dehydrated by exposing them to 50%, 60%, 70%, 80%, 90% and100% ethanol for 15 minutes each. The sample was dried in a critical point dryer before SEM imaging was performed.

Fluorescence staining

For fluorescence staining, substrates were gently rinsed with PBS at room temperature. Calcein AM (Thermo Fisher Scientific) and Hoechst 33342 (Thermo Fisher Scientific) were diluted in PBS. The dye mixture was added to the culture dish, using just enough to cover the substrates and left at room temperature in the dark for 20 minutes. Post staining substrates were washed with PBS and imaged using a fluorescence microscope. The BoM cells were also stained by Calcein AM for imaging.

Imaging

Fluorescence images were obtained using a Leica microscope with a 10x objective. For imaging of cells expressing tdTomato fluorescent protein, or stained with Calcein and Hoechst, red, green and blue filters were used, respectively. For high-resolution fluorescence imaging, a Leica SP8 confocal microscope with a 40X water immersion objective was used.

Image analysis

ImageJ software was used for the analysis of fluorescence images. A cell counter plugin was used within the ImageJ software for counting the cells in the live/dead assay. Contact angle of a water droplet on the Au/SiNW substrate was also measured in ImageJ.

Shape mode analysis

For the shape mode analysis, the fluorescence images were segmented using CellProfiler[63]. The segmented cells were then subjected to VAMPIRE (Visually Aided Morpho-Phenotyping Image Recognition) analysis[59,60]. In this analysis, the images were rotationally aligned, and boundary coordinate points were extracted. Thereafter, principal component analysis was applied on the shape-coordinates and different shape modes were extracted. Every cell was then represented as a weighted sum of different shape modes. The cells were finally binned to a shape mode that carried the maximum weight. Cell spreading was calculated by dividing the average area of cells on Au/NWs by that on Si. 1.39-fold elongation was calculated by dividing the aspect ratio (major axis/minor axis: fitting the cell to an ellipse) of cells on Au/NWs by that on Si. Circularity was calculated using the formula $(4*pi*area)/(perimeter)^2$. The area, aspect ratio and circularity were averaged over 300 cells with shape modes 5 and 6 for Au/SiNWs substrates and shape mode 3 for Si.

Supplementary Material

Refer to Web version on PubMed Central for supplementary material.

Acknowledgements

This work is supported by the Italian Minister of Foreign Affairs and International Collaboration (MAECI) under the Joint research project “Scalable nano-plasmonic platform for differentiation and drug response monitoring of organ-tropic metastatic cancer cells” (US19GR07) within the Scientific and Collaboration Program Italy-USA/ 2019-2021. D.P. and I.B. acknowledge support from National Institute of Biomedical Imaging and Bioengineering (2-P41-EB015871-31) and National Institute of General Medical Sciences (DP2GM128198). K.G. acknowledges support from the National Cancer Institute (R01 CA213428, R01 CA213492).

References:

1. Berrier AL, and Yamada KM (2007) Cell-matrix adhesion. J. Cell. Physiol, 213 (3), 565–573. [PubMed: 17680633]
2. Rosso F, Giordano A, Barbarisi M, and Barbarisi A (2004) From cell-ECM interactions to tissue engineering. J. Cell. Physiol, 199 (2), 174–180. [PubMed: 15039999]
3. Vining KH, and Mooney DJ (2017) Mechanical forces direct stem cell behaviour in development and regeneration. Nat. Rev. Mol. Cell Biol, 18 (12), 728–742. [PubMed: 29115301]
4. Ladoux B, and Mège R-M (2017) Mechanobiology of collective cell behaviours. Nat. Rev. Mol. Cell Biol, 18 (12), 743–757. [PubMed: 29115298]
5. Upadhyaya A (2017) Mechanosensing in the immune response. Seminars in Cell & Developmental Biology, 71, 137–145. [PubMed: 28830744]
6. Timpl R (1989) Structure and biological activity of basement membrane proteins. EJB Reviews 1989, 13–28.
7. Yurchenco PD, and Schittny JC (1990) Molecular architecture of basement membranes. FASEB J, 4 (6), 1577–1590. [PubMed: 2180767]
8. Abrams G, Teixeira A, Nealey P, and Murphy C (2002) Effects of Substratum Topography on Cell Behavior. Biomimetic Materials And Design.
9. Flemming RG, Murphy CJ, Abrams GA, Goodman SL, and Nealey PF (1999) Effects of synthetic micro- and nano-structured surfaces on cell behavior. Biomaterials, 20 (6), 573–588. [PubMed: 10213360]
10. Karuri NW, Liliensiek S, Teixeira AI, Abrams G, Campbell S, Nealey PF, and Murphy CJ (2004) Biological length scale topography enhances cell-substratum adhesion of human corneal epithelial cells. J. Cell Sci, 117 (Pt 15), 3153–3164. [PubMed: 15226393]
11. Tian B, Liu J, Dvir T, Jin L, Tsui JH, Qing Q, Suo Z, Langer R, Kohane DS, and Lieber CM (2012) Macroporous nanowire nanoelectronic scaffolds for synthetic tissues. Nat. Mater, 11 (11), 986–994. [PubMed: 22922448]
12. Liu X, and Wang S (2014) Three-dimensional nano-biointerface as a new platform for guiding cell fate. Chem. Soc. Rev, 43 (8), 2385–2401. [PubMed: 24504119]
13. Kishore V, Bullock W, Sun X, Van Dyke WS, and Akkus O (2012) Tenogenic differentiation of human MSCs induced by the topography of electrochemically aligned collagen threads. Biomaterials, 33 (7), 2137–2144. [PubMed: 22177622]
14. Younesi M, Islam A, Kishore V, Anderson JM, and Akkus O (2014) Tenogenic Induction of Human MSCs by Anisotropically Aligned Collagen Biotextiles. Adv. Funct. Mater, 24 (36), 5762–5770. [PubMed: 25750610]
15. Barros D, Parreira P, Furtado J, Ferreira-da-Silva F, Conde-Sousa E, García AJ, Martins MCL, Amaral IF, and Pêgo AP (2019) An affinity-based approach to engineer laminin-presenting cell instructive microenvironments. Biomaterials, 192, 601–611. [PubMed: 30509501]
16. Baker BM, and Chen CS (2012) Deconstructing the third dimension: how 3D culture microenvironments alter cellular cues. J. Cell Sci, 125 (Pt 13), 3015–3024. [PubMed: 22797912]
17. Théry M, Jiménez-Dalmaroni A, Racine V, Bornens M, and Jülicher F (2007) Experimental and theoretical study of mitotic spindle orientation. Nature, 447 (7143), 493–496. [PubMed: 17495931]
18. Whitesides GM, Ostuni E, Takayama S, Jiang X, and Ingber DE (2001) Soft lithography in biology and biochemistry. Annu. Rev. Biomed. Eng, 3, 335–373. [PubMed: 11447067]
19. Salaita K, Nair PM, Petit RS, Neve RM, Das D, Gray JW, and Groves JT (2010) Restriction of receptor movement alters cellular response: physical force sensing by EphA2. Science, 327 (5971), 1380–1385. [PubMed: 20223987]
20. Mrksich M (2000) A surface chemistry approach to studying cell adhesion. Chemical Society Reviews, 29 (4), 267–273.
21. Pêgo AP, Vleggeert-Lankamp CLAM, Deenen M, Lakke EAJF, Grijpma DW, Poot AA, Marani E, and Feijen J (2003) Adhesion and growth of human Schwann cells on trimethylene carbonate (co)polymers. J. Biomed. Mater. Res. A, 67 (3), 876–885. [PubMed: 14613236]

22. Raucci MG, Alvarez-Perez MA, Demitri C, Sannino A, and Ambrosio L (2012) Proliferation and osteoblastic differentiation of hMSCs on cellulose-based hydrogels. J. Appl. Biomater. Funct. Mater, 10 (3), 302–307. [PubMed: 23242882]
23. Dowling DP, Miller IS, Ardhaoui M, and Gallagher WM (2011) Effect of surface wettability and topography on the adhesion of osteosarcoma cells on plasma-modified polystyrene. J. Biomater. Appl, 26 (3), 327–347. [PubMed: 20566655]
24. Ranella A, Barberoglou M, Bakogianni S, Fotakis C, and Stratakis E (2010) Tuning cell adhesion by controlling the roughness and wettability of 3D micro/nano silicon structures. Acta Biomater, 6 (7), 2711–2720. [PubMed: 20080216]
25. Bettinger CJ, Langer R, and Borenstein JT (2009) Engineering substrate topography at the micro- and nanoscale to control cell function. Angew. Chem. Int. Ed Engl, 48 (30), 5406–5415. [PubMed: 19492373]
26. Martínez E, Engel E, Planell JA, and Samitier J (2009) Effects of artificial micro- and nano-structured surfaces on cell behaviour. Ann. Anat, 191 (1), 126–135. [PubMed: 18692370]
27. Elnathan R, Kwiat M, Patolsky F, and Voelcker NH (2014) Engineering vertically aligned semiconductor nanowire arrays for applications in the life sciences. Nano Today, 9 (2), 172–196.
28. Bonde S, Buch-Månson N, Rostgaard KR, Andersen TK, Berthing T, and Martinez KL (2014) Exploring arrays of vertical one-dimensional nanostructures for cellular investigations. Nanotechnology, 25 (36), 362001. [PubMed: 25130133]
29. Na Y-R, Kim SY, Gaublomme JT, Shalek AK, Jorgolli M, Park H, and Yang EG (2013) Probing Enzymatic Activity inside Living Cells Using a Nanowire–Cell “Sandwich” Assay. Nano Letters, 13 (1), 153–158. [PubMed: 23244056]
30. Choi S, Kim H, Kim SY, and Yang EG (2016) Probing protein complexes inside living cells using a silicon nanowire-based pull-down assay. Nanoscale, 8 (22), 11380–11384. [PubMed: 27198202]
31. Xu AM, Aalipour A, Leal-Ortiz S, Mekhdjian AH, Xie X, Dunn AR, Garner CC, and Melosh NA (2014) Quantification of nanowire penetration into living cells. Nat. Commun, 5, 3613. [PubMed: 24710350]
32. Kim W, Ng JK, Kunitake ME, Conklin BR, and Yang P (2007) Interfacing silicon nanowires with mammalian cells. J. Am. Chem. Soc, 129 (23), 7228–7229. [PubMed: 17516647]
33. Robinson JT, Jorgolli M, Shalek AK, Yoon M-H, Gertner RS, and Park H (2012) Vertical nanowire electrode arrays as a scalable platform for intracellular interfacing to neuronal circuits. Nat. Nanotechnol, 7 (3), 180–184. [PubMed: 22231664]
34. Xie C, Lin Z, Hanson L, Cui Y, and Cui B (2012) Intracellular recording of action potentials by nanopillar electroporation. Nat. Nanotechnol, 7 (3), 185–190. [PubMed: 22327876]
35. Hällström W, Lexholm M, Suyatin DB, Hammarin G, Hessman D, Samuelson L, Montelius L, Kanje M, and Prinz CN (2010) Fifteen-piconewton force detection from neural growth cones using nanowire arrays. Nano Lett, 10 (3), 782–787. [PubMed: 20102185]
36. Qing Q, Jiang Z, Xu L, Gao R, Mai L, and Lieber CM (2014) Free-standing kinked nanowire transistor probes for targeted intracellular recording in three dimensions. Nat. Nanotechnol, 9 (2), 142–147. [PubMed: 24336402]
37. Li Y, Wei Y, Liao J, Hao Y, Ning C, Jiang L, and Wang S (2016) Surface Wettability Switched Cell Adhesion and Detachment on Conducting Polymer Nanoarray. Advanced Materials Interfaces, 3 (19), 1600598.
38. Geyer FL, Ueda E, Liebel U, Grau N, and Levkin PA (2011) Superhydrophobic-superhydrophilic micropatterning: towards genome-on-a-chip cell microarrays. Angew. Chem. Int. Ed Engl, 50 (36), 8424–8427. [PubMed: 21751312]
39. Piret G, Galopin E, Coffinier Y, Boukherroub R, Legrand D, and Slomianny C (2011) Culture of mammalian cells on patterned superhydrophilic/superhydrophobic silicon nanowire arrays. Soft Matter, 7 (18), 8642.
40. Abrams GA, Goodman SL, Nealey PF, Franco M, and Murphy CJ (2000) Nanoscale topography of the basement membrane underlying the corneal epithelium of the rhesus macaque. Cell Tissue Res, 299 (1), 39–46. [PubMed: 10654068]

41. Nicolas J, Magli S, Rabbachin L, Sampaolesi S, Nicotra F, and Russo L (2020) 3D Extracellular Matrix Mimics: Fundamental Concepts and Role of Materials Chemistry to Influence Stem Cell Fate. Biomacromolecules, 21 (6), 1968–1994. [PubMed: 32227919]
42. Saracino E, Maiolo L, Polese D, Semprini M, Borrachero-Conejo AI, Gasparetto J, Murtagh S, Sola M, Tomasi L, Valle F, Pazzini L, Formaggio F, Chiappalone M, Hussain S, Caprini M, Muccini M, Ambrosio L, Fortunato G, Zamboni R, Convertino A, and Benfenati V (2020) A Glial-Silicon Nanowire Electrode Junction Enabling Differentiation and Noninvasive Recording of Slow Oscillations from Primary Astrocytes. Advanced Biosystems, 4 (4), 1900264.
43. Convertino A, Mussi V, Maiolo L, Ledda M, Lolli MG, Bovino FA, Fortunato G, Rocchia M, and Lisi A (2018) Array of disordered silicon nanowires coated by a gold film for combined NIR photothermal treatment of cancer cells and Raman monitoring of the process evolution. Nanotechnology, 29 (41), 415102. [PubMed: 30059014]
44. Maiolo L, Polese D, Pecora A, Fortunato G, Shacham-Diamand Y, and Convertino A (2016) Highly Disordered Array of Silicon Nanowires: an Effective and Scalable Approach for Performing and Flexible Electrochemical Biosensors. Adv. Healthc. Mater, 5 (5), 575–583. [PubMed: 26717420]
45. Rizwan A, Paidi SK, Zheng C, Cheng M, Barman I, and Glunde K (2018) Mapping the genetic basis of breast microcalcifications and their role in metastasis. Sci. Rep, 8 (1), 11067. [PubMed: 30038419]
46. Liu Z, Lee SJ, Park S, Konstantopoulos K, Glunde K, Chen Y, and Barman I (2020) Cancer cells display increased migration and deformability in pace with metastatic progression. FASEB J, 34 (7), 9307–9315. [PubMed: 32463148]
47. Paidi SK, Shah V, Raj P, Glunde K, Pandey R, and Barman I (2020) Coarse Raman and optical diffraction tomographic imaging enable label-free phenotyping of isogenic breast cancer cells of varying metastatic potential. Biosens. Bioelectron, 112863. [PubMed: 33272866]
48. Winkler J, Abisoye-Ogunniyan A, Metcalf KJ, and Werb Z (2020) Concepts of extracellular matrix remodelling in tumour progression and metastasis. Nat. Commun, 11 (1), 5120. [PubMed: 33037194]
49. Wirtz D, Konstantopoulos K, and Searson PC (2011) The physics of cancer: the role of physical interactions and mechanical forces in metastasis. Nat. Rev. Cancer, 11 (7), 512–522. [PubMed: 21701513]
50. Zhou Z-H, Ji C-D, Xiao H-L, Zhao H-B, Cui Y-H, and Bian X-W (2017) Reorganized Collagen in the Tumor Microenvironment of Gastric Cancer and Its Association with Prognosis. J. Cancer, 8 (8), 1466–1476. [PubMed: 28638462]
51. Levental KR, Yu H, Kass L, Lakins JN, Egeblad M, Erler JT, Fong SFT, Csiszar K, Giaccia A, Weninger W, Yamauchi M, Gasser DL, and Weaver VM (2009) Matrix crosslinking forces tumor progression by enhancing integrin signaling. Cell, 139 (5), 891–906. [PubMed: 19931152]
52. Venning FA, Wullkopf L, and Erler JT (2015) Targeting ECM Disrupts Cancer Progression. Front. Oncol, 5, 224. [PubMed: 26539408]
53. Psaila B, and Lyden D (2009) The metastatic niche: adapting the foreign soil. Nature Reviews Cancer, 9 (4), 285–293. [PubMed: 19308068]
54. Dalby MJ, Riehle MO, Yarwood SJ, Wilkinson CDW, and Curtis ASG (2003) Nucleus alignment and cell signaling in fibroblasts: response to a micro-grooved topography. Exp. Cell Res, 284 (2), 274–282. [PubMed: 12651159]
55. Teixeira AI, Nealey PF, and Murphy CJ (2004) Responses of human keratocytes to micro- and nanostructured substrates. J. Biomed. Mater. Res. A, 71 (3), 369–376. [PubMed: 15470741]
56. Azatov M, Sun X, Suberi A, Fourkas JT, and Upadhyaya A (2017) Topography on a subcellular scale modulates cellular adhesions and actin stress fiber dynamics in tumor associated fibroblasts. Phys. Biol, 14 (6), 065003. [PubMed: 28635615]
57. Teixeira AI, McKie GA, Foley JD, Bertics PJ, Nealey PF, and Murphy CJ (2006) The effect of environmental factors on the response of human corneal epithelial cells to nanoscale substrate topography. Biomaterials, 27 (21), 3945–3954. [PubMed: 16580065]
58. Clark P, Connolly P, Curtis AS, Dow JA, and Wilkinson CD (1990) Topographical control of cell behaviour: II. Multiple grooved substrata. Development, 108 (4), 635–644. [PubMed: 2387239]

59. Wu P-H, Phillip JM, Khatau SB, Chen W-C, Stirman J, Rosseel S, Tschudi K, Van Patten J, Wong M, Gupta S, Baras AS, Leek JT, Maitra A, and Wirtz D (2015) Evolution of cellular morpho-phenotypes in cancer metastasis. Sci. Rep, 5, 18437. [PubMed: 26675084]

60. Phillip JM, Han K-S, Chen W-C, Wirtz D, and Wu P-H (2021) A robust unsupervised machine-learning method to quantify the morphological heterogeneity of cells and nuclei. Nat. Protoc

61. Rapisarda M, Simeone D, Fortunato G, Valletta A, and Mariucci L (2011) Pentacene thin film transistors with (polytetrafluoroethylene) PTFE-like encapsulation layer. Organic Electronics, 12 (1), 119–124.

62. Minn AJ, Kang Y, Serganova I, Gupta GP, Giri DD, Doubrovin M, Ponomarev V, Gerald WL, Blasberg R, and Massagué J (2005) Distinct organ-specific metastatic potential of individual breast cancer cells and primary tumors. J. Clin. Invest, 115 (1), 44–55. [PubMed: 15630443]

63. McQuin C, Goodman A, Chernyshev V, Kamentsky L, Cimini BA, Karhohs KW, Doan M, Ding L, Rafelski SM, Thirstrup D, Wiegraebe W, Singh S, Becker T, Caicedo JC, and Carpenter AE (2018) CellProfiler 3.0: Next-generation image processing for biology. PLoS Biol, 16 (7), e2005970. [PubMed: 29969450]

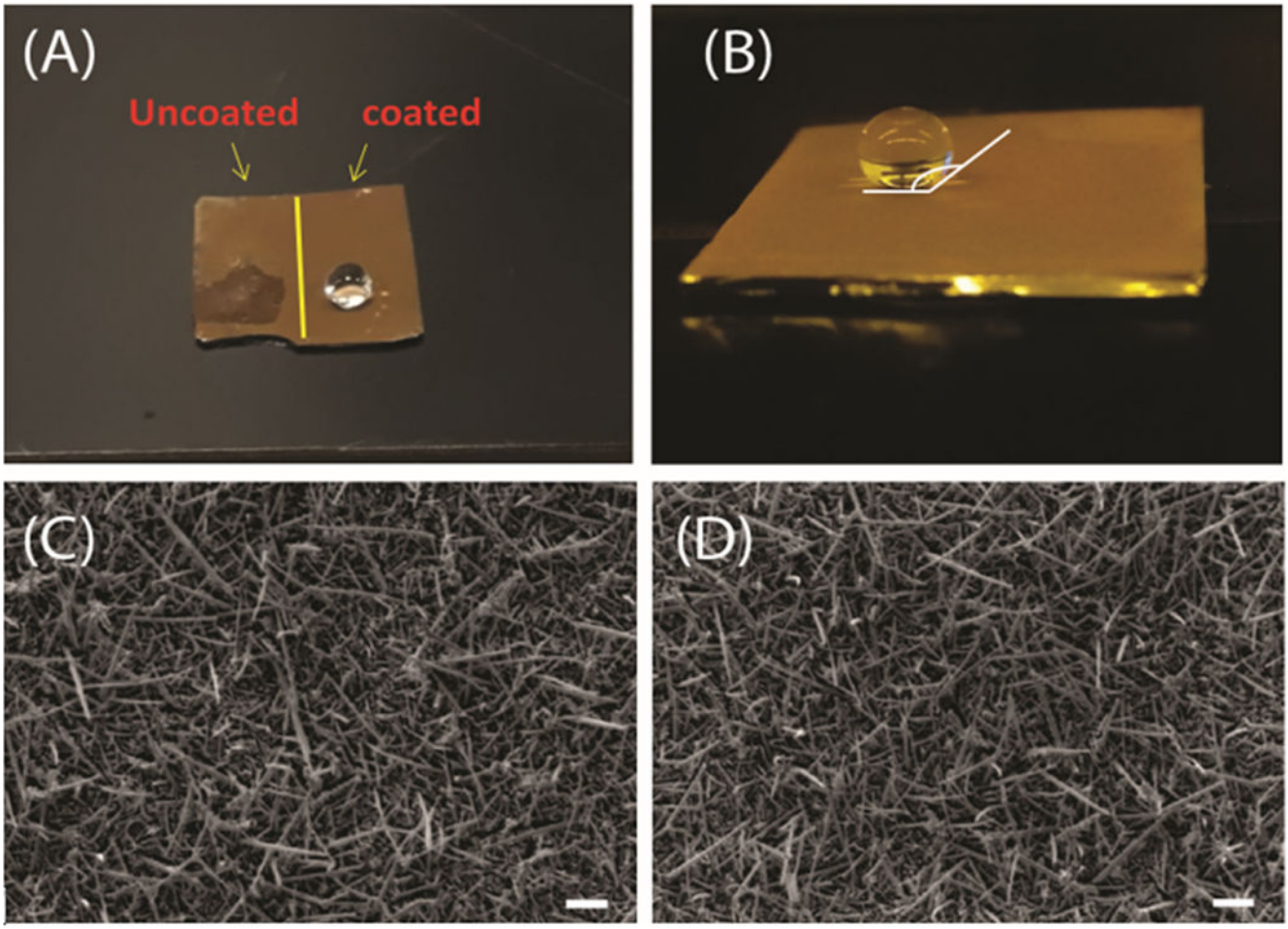

Figure 1.

(A) Photograph of the wettability difference between pristine and CHF_3 treated regions on the same Au/SiNWs substrate. (B) Contact angle on the super-hydrophobic surface is 155°. (C) and (D) are SEM images of pristine Au/SiNWs and after CHF_3 treatment, respectively. Scale bar 1 μm.

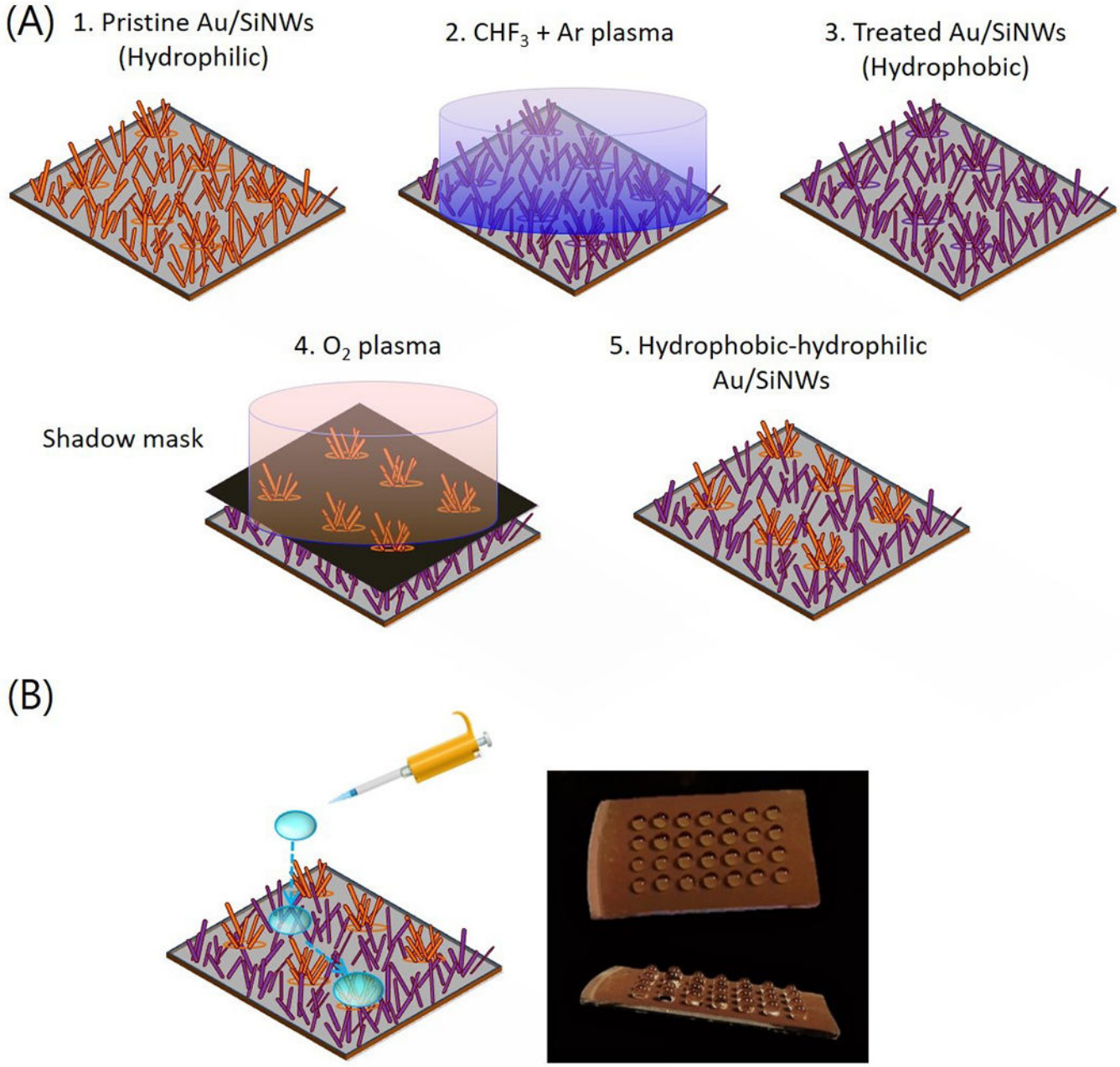

Figure 2.

(A) Schematic of the workflow of fabricating hydrophobic-hydrophilic patterned Au/SiNWs. (B) Schematic illustration of the hydrophilic/hydrophobic mesh on the substrate. A water droplet easily rolls to a hydrophilic region. Photographs of the water droplets immobilized onto the hydrophilic islands of the patterned hydrophilic/hydrophobic substrate.

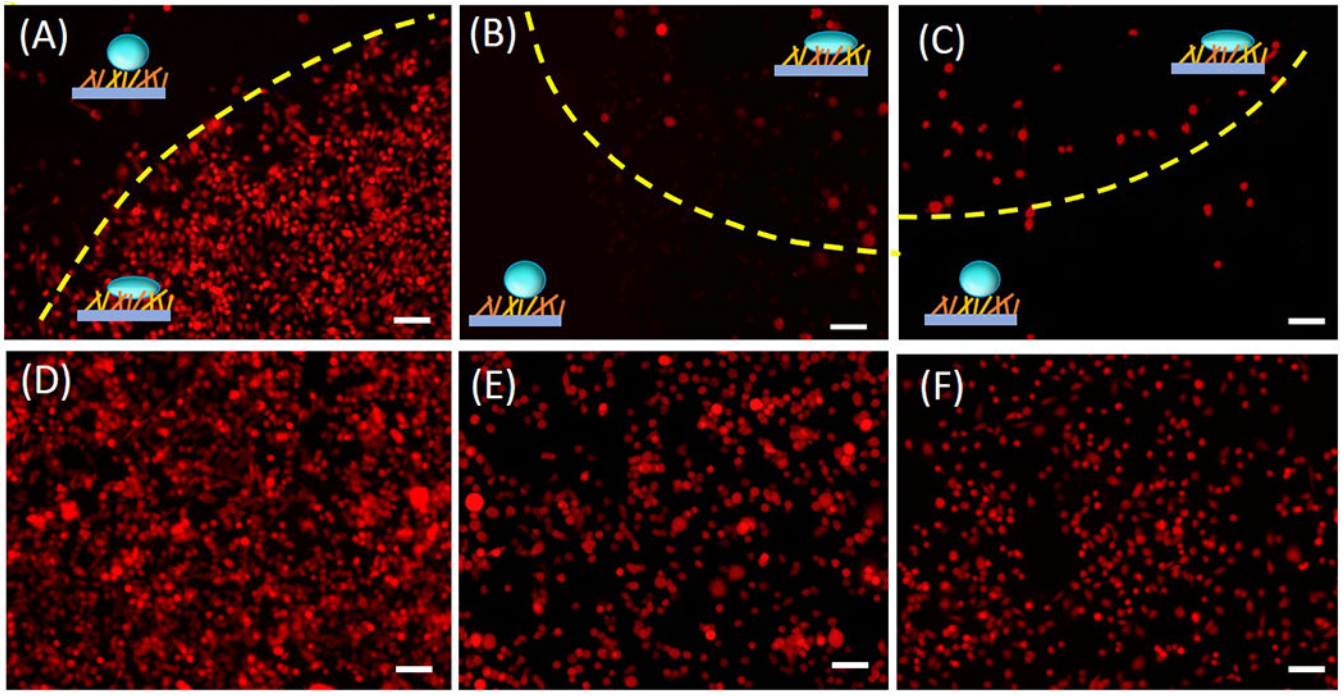

Figure 3.

(A)-(C) Fluorescence image of P231, LM231 and BoM cells on hydrophobic-hydrophilic Au/SiNWs observed after 2 days of plating on the substrate. The yellow dashed line demarcates the hydrophilic and the hydrophobic region, which are also marked with schematic representations. (D)-(F) Fluorescence image of the P231, LM231 and BoM cells on a flat surface used as a control. Scale Bar 100 μm.

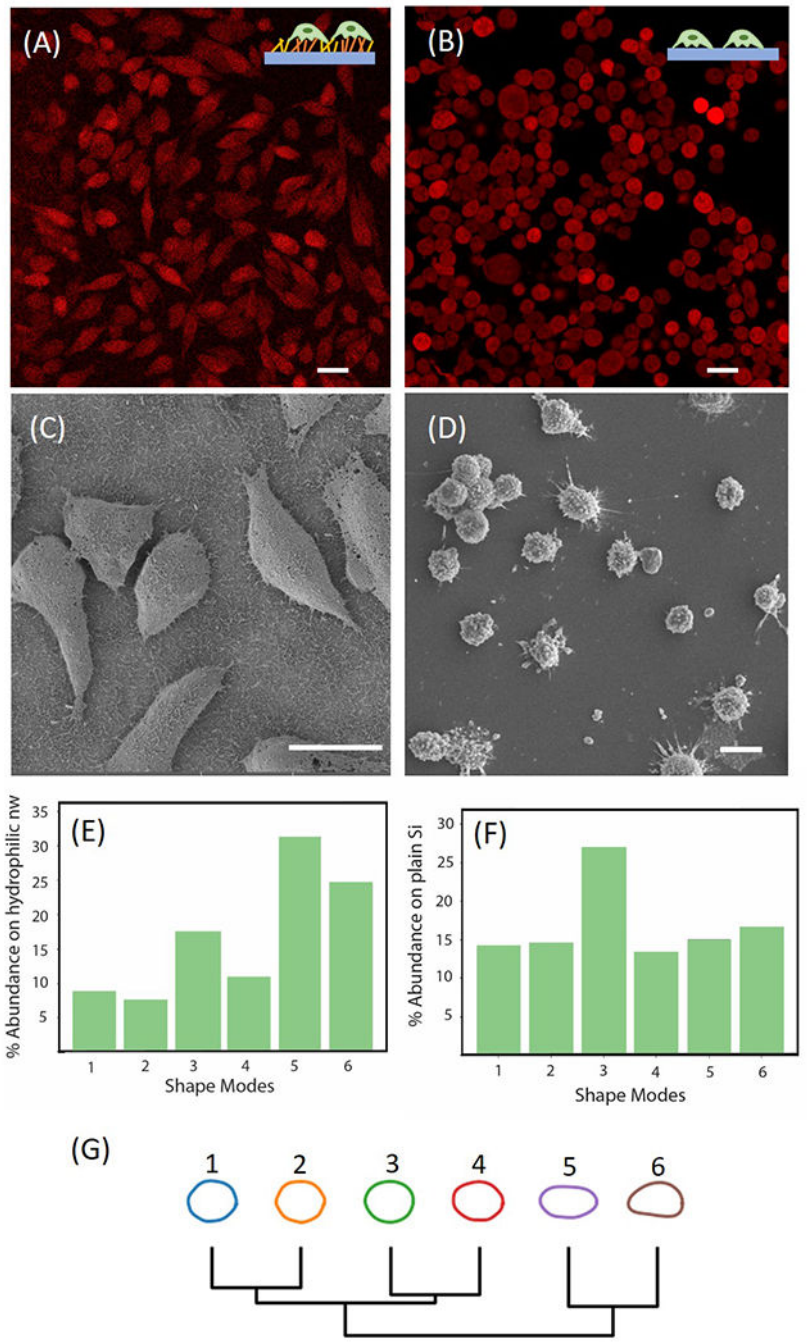

Figure 4.

(A) Fluorescence image of parental P231 cells on patterned Au/SiNWs. (B) Fluorescence image of parental P231 cells on plain Si wafer. Scale Bar 20 μm. (C) SEM image of P231 cells on the hydrophilic region of the Au/SiNWs substrate. (D) SEM image of P231 cells on flat surface. Scale bar 20 μm. (E) Distribution of various shape modes of parental P231 cells on Au/SiNWs using VAMPIRE analysis. (F) Distribution of various shape modes of parental P231 cells on plain Si wafer using VAMPIRE analysis. (G) Dendrogram of various shape modes showing the relation between each mode.

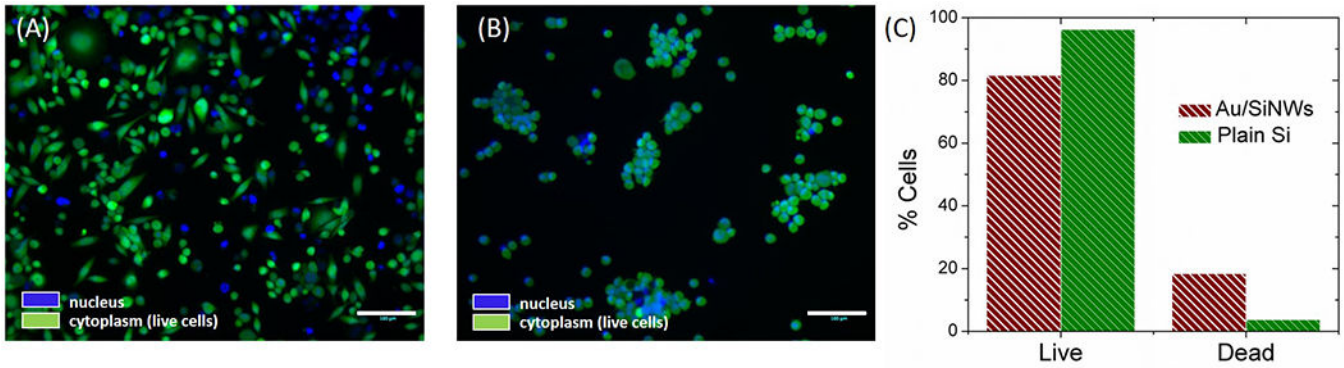

Figure 5.

Cell viability. (A) Merged fluorescence image of live-dead assay of P231 cells on Au/SiNWs after 24 hours of plating. The nuclei of all cells (irrespective if alive or dead) was stained by Hoechst 33342 and has a blue emission (represented by blue color in the image) and the cytoplasm of live cells was stained by Calcein AM with emission in the green (represented by green in the figure). In the overlay image, the bright blue color of nuclei was brighter in dead cells whose cytoplasm was not stained by Calcein. (B) Merged fluorescence image of live-dead assay on plain Si wafer. Scale bar 100 μm. (C) Bar graph representation of percentage of live and dead cells on Au/SiNWs as compared to plain Si.